Corrosion Science 52 (2010) 1696–1704

Contents lists available at ScienceDirect

Corrosion Science

journal homepage: www.elsevier.com/locate/corsci

Influence of chloride ion concentration and temperature on the corrosion of Mg–Al alloys in salt fog

M.C. Merino [a], A. Pardo [a], R. Arrabal [a,*], S. Merino [b], P. Casajús [a], M. Mohedano [a]

[a] Departamento de Ciencia de Materiales, Facultad de Química, Universidad Complutense, 28040 Madrid, Spain
[b] Departamento de Tecnología Industrial, Universidad Alfonso X El Sabio, 28691, Villanueva de la Cañada, Madrid, Spain

ARTICLE INFO

Article history:
Received 14 September 2009
Accepted 16 January 2010
Available online 22 January 2010

Keywords:
A. Magnesium
B. Atmospheric corrosion
C. Weight loss

ABSTRACT

The influence of temperature and chloride concentration on the corrosion behaviour of Mg–Al alloys exposed to salt fog was evaluated. Corrosion attack increased with decreasing aluminium content in the alloy and increasing Cl^- concentration and temperature. The effect of Al–Mn inclusions, which revealed several stoichiometries and were up to 300 mV more noble than the magnesium matrix, was only noticeable in the early stages of corrosion of the AZ31 alloy. Aluminium segregation and β-phase distribution were the main controlling factors for the AZ80 and AZ91D alloys, the latter being more susceptible to variations in the saline concentration.

1. Introduction

Magnesium is now becoming the material of choice for many lightweight transport component applications due to its combination of low density and excellent physical and mechanical properties; demonstrated by continued and steady market growth over the past 10 years. In the alloyed form, magnesium is the lightest structural metal and is a potential candidate to replace heavier aluminium or steel components, reducing fuel consumption and harmful emissions in the transport sector [1]. However, the use of magnesium alloys for structural applications has limited success due to their poor corrosion properties [2–7].

Aluminium is the most important alloying element for magnesium. A large number of studies have been carried out in order to assess the effect of aluminium content, casting shape, thermal treatment and alloy microstructure on the corrosion behaviour of Mg–Al alloys immersed in chloride-containing solutions [8]. Increasing aluminium content in Mg–Al alloys normally results in better corrosion behaviour, but the specific mechanism and influence of aluminium is still not clear. For the majority of Mg–Al alloys, aluminium is partly in solid solution and partly precipitated along the grain boundaries in the form of $Mg_{17}Al_{12}$ (β-phase). Some studies claim that if the β-phase forms a finely divided and continuous network it may act as barrier to inhibit the overall corrosion of the alloy [9]. It has also been suggested that an increase in the relative size of the β-phase at the expense of the Al-rich-α area, increasing the cathode to anode area ratio, results in greater localized corrosion [10]. Thus, the corrosion of Mg–Al alloys is greatly influenced by the aluminium distribution and morphology of the β-phase, which typically forms micro-galvanic couples with other phases [11].

In dry environments, magnesium has good resistance to oxidation or corrosion at normal ambient temperature [12]. However, in high humidity environments, moisture can lead to rapid surface degradation, which is much more noticeable in the presence of Cl^- ions [13,14]. The temperature and ambient concentrations of CO_2 also have an effect on the atmospheric corrosion resistance of magnesium alloys. Normally, corrosion rate increases as temperature increases, whereas CO_2 has a beneficial effect due to the formation of slightly protective films consisting of magnesium carbonates [15]. Corrosion behaviour of magnesium alloys under atmospheric conditions differs considerably from exposure to aqueous solutions [16]. According to Tomashov [17], the main cathodic reaction in aqueous solution is water reduction, but during atmospheric corrosion with thin electrolyte layers, the oxygen reduction is the main reaction. Therefore, the effect of several factors such as chloride ion concentration, temperature, and alloy microstructure can be quite different to that observed during immersion tests.

In the present study the influence of Al content, alloy microstructure, chloride concentration and temperature on the corrosion behaviour of the AZ31, AZ80 and AZ91D magnesium alloys was evaluated by accelerated laboratory tests in a salt fog cabinet [18].

2. Experimental

2.1. Test materials

The studied materials were AZ31, AZ80 and AZ91D magnesium alloys and commercially pure or "low-purity" Mg as the reference

* Corresponding author. Tel.: +34 91 3945227; fax: +34 91 3944357.
E-mail address: raularrabal@quim.ucm.es (R. Arrabal).

0010-938X/$ - see front matter © 2010 Elsevier Ltd. All rights reserved.
doi:10.1016/j.corsci.2010.01.020

Table 1
Chemical composition of the test materials.

Material	Elements (wt.%)									
	Al	Zn	Mn	Si	Cu	Fe	Ni	Ca	Zr	Others
Mg 99.9%	0.006	0.014	0.03	0.019	0.001	0.004	<0.001			
AZ31	3.1	0.73	0.25	0.02	<0.001	0.005	<0.001	<0.01	<0.001	<0.30
AZ80	8.2	0.46	0.13	0.01	<0.001	0.004				<0.30
AZ91D	8.8	0.68	0.30	0.01	<0.001	0.004	<0.008			<0.30

Table 2
Salt fog conditions.

Maximum exposure time (days)	21
pH	6.5–7.2
Atomized air pressure (kN m^{-2})	69–172
Temperature (°C)	20
	35
NaCl (wt.%)	2
	3.5
	5

material. Mg and AZ31 materials were fabricated in wrought condition and supplied in plates of 3 mm thickness, whereas AZ80 and AZ91D alloys were manufactured by a casting process in the form of billets of 300 and 250 mm in diameter. All the materials were supplied by Magnesium Elektron Ltd. The chemical compositions of the tested magnesium materials are listed in Table 1.

2.2. Specimen examination

For metallographic characterization, samples were wet ground through successive grades of silicon carbide abrasive papers from P120 to P2000, followed by diamond finishing to 0.1 μm. Two etching reagents were used: (a) 5% Nital (5 mL HNO_3 + 95 mL ethanol), to reveal the constituents and general microstructure of Mg, AZ80 and AZ91D materials and (b) Vilella reagent (0.6 g picric acid + 10 mL ethanol + 90 mL H_2O), to reveal grain boundaries in the AZ31 alloy. The constituents were examined by scanning electron microscope (SEM) using a JEOL JSM-6400 microscope equipped with Oxford Link energy-dispersive X-ray (EDX) microanalysis hardware. The corrosion products were removed in boiling chromium trioxide (200 g L^{-1}) solution during 1 min for characterization of the initial stages of corrosion of the Mg–Al alloys. For low angle X-ray diffraction (XRD) studies, a Philips X'Pert diffractometer ($K_\alpha Cu$ = 1.54056 Å) was used.

Extraction of carbon replicas was used for characterization of Al–Mn particles imbedded in the studied Mg–Al alloys. The carbon extraction replicas were examined in a JEOL 2000-FX transmission electron microscope (TEM) operating at 200 kV and equipped with Oxford link EDX microanalysis hardware.

Surface potential maps of polished specimens were obtained using a MultiMode scanning probe microscope (Veeco-Digital Instruments) working in tapping mode and using a silicon tip with a platinum-coating of 20 nm thickness as the reference electrode. All measurements were made at room temperature with a relative humidity in the range of 40–65%.

2.3. Gravimetric measurements

Prior to the corrosion tests, specimens with a working area of 16 cm^2 were wet ground to a P1200 SiC finish, followed by rinsing with isopropyl alcohol in an ultrasonic bath and drying in warm air.

The specimens were hung in a climatic cabinet with a nylon thread and exposed to salt fog according to ASTM B 117 standard. Test conditions are given in Table 2. At the end of the tests, the specimens were washed with hot water (<38 °C) in order to remove saline deposits formed on the material surfaces and then

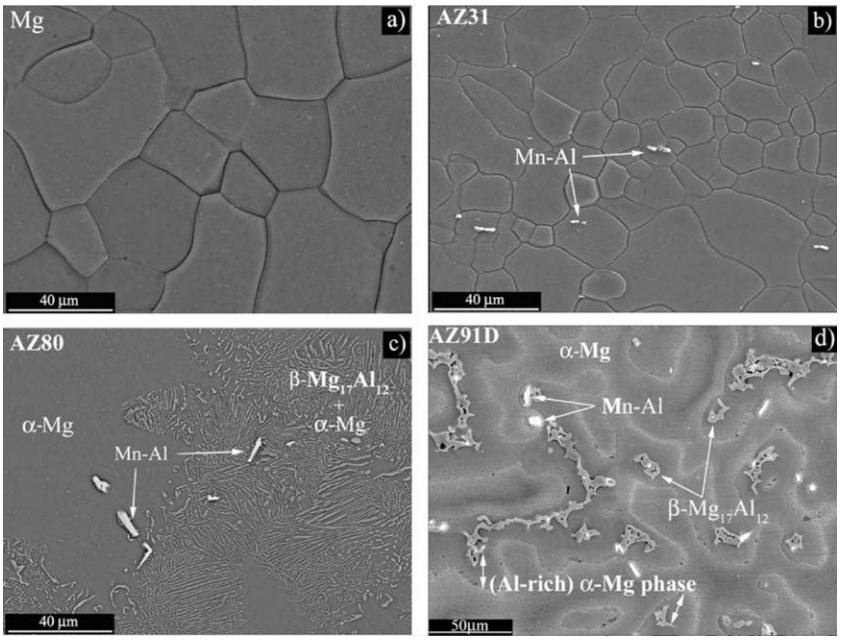

Fig. 1. Backscattered scanning electron (BSE) micrographs of (a) Mg, (b) AZ31, (c) AZ80 and (d) AZ91D.

dried with hot air. Mass changes per unit of surface area were calculated from the expression $(M_i - M_f)/A$, where M_i is the initial mass, M_f the final mass and A the exposed surface area. Samples were weighed using a Sartorius BP 211D scale with a precision of 0.00001 g. In all cases, tests were performed in duplicate to guarantee the reliability of the results.

2.4. Characterization of corrosion products

The specimens were examined by SEM, EDX and XRD in order to study the influence of Al content and alloy microstructure on the morphology of the corrosion attack and composition of the corrosion products.

3. Results

3.1. Materials characterization

3.1.1. Sem

Fig. 1 shows the backscattered scanning electron (BSE) micrographs of Mg, AZ31, AZ80 and AZ91D materials. Unalloyed Mg reveals equiaxial grains with an average size of 45 μm (Fig. 1a). In the AZ31 alloy, the grain size is in the range of 5–100 μm (Fig. 1b). The AZ80 alloy reveals α-Mg grains (~100 μm) and grains (100–200 μm) with discontinuous precipitation of a fine lamellar aggregate (α-Mg + β-$Mg_{17}Al_{12}$) (Fig. 1c). The AZ91D alloy shows α-Mg primary dendrites and eutectic α-Mg/$Mg_{17}Al_{12}$ in the interdendritic regions, which is in partially divorced form with respect to solid solution (Fig. 1d). Al–Mn second phase particles were found for the AZ31, AZ80 and AZ91D alloys inside the grains and at grain boundaries.

3.1.2. Tem

The crystalline structure and composition of Al–Mn inclusions were determined by TEM and EDX analysis respectively. Fig. 2a–c show that the majority of Al–Mn particles have an angular blocky morphology with a size in the interval of 1–15 μm. The particles sometimes have irregular, saw-tooth surfaces, which result from growth in the mushy and early solid stages [19]. EDX analysis of Al–Mn particles obtained from carbon extraction replicas of the AZ31 alloy indicated an average composition (in wt.%) of 46.3Al–53.0Mn–0.7Fe. For the AZ80 and AZ91D alloys, the average compositions were 49.5Al–49.8Mn–0.7Fe and 42.1Al–56.7Mn–1.2Fe, respectively. Iron content in the Al–Mn particles oscillated from 0 to 2.5 wt.%. According to the Al–Mn phase diagram, the Al/Mn ratios suggested particles of the Al_8Mn_5 type. Electron diffraction patterns, illustrated in Fig. 2, also revealed the presence of Al–Mn particles containing lower Mn concentrations. Table 3 shows the Al–Mn particles identified in the studied alloys.

3.1.3. Surface potential

Fig. 3 shows topographic images and surface potential profiles of the AZ31, AZ80 and AZ91D alloys. These results provided information about the local nobility of different microstructural phases on a submicron scale [20–23]. For all three Mg–Al alloys, Al–Mn particles presented a cathodic behaviour, with potential values up to 300 mV higher than the surrounding magnesium matrix. For the AZ80 and AZ91D alloys, the potential difference between the β-phase and the surrounding material was found to be ~50–100 mV. This difference is smaller than the one found for the die-cast AZ91D alloy in [24], which was about 200 mV. This discrepancy is possibly associated with the different microstructure of the alloys and local variations in the composition of the intermetallic phases. Thus, in [24] a die-cast alloy was examined, whereas as-cast AZ80 and AZ91D alloys were used in the present study. Despite the previous, from the surface potential maps, it is clear that the β-$Mg_{17}Al_{12}$ phase and the Al–Mn particles act as local cathodes when coupled to the α-Mg phase. The surface coverage of the β-phase is much higher than that of the Al–Mn particles and this first phase should play a more important role in the corrosion of the AZ80 and AZ91D alloys.

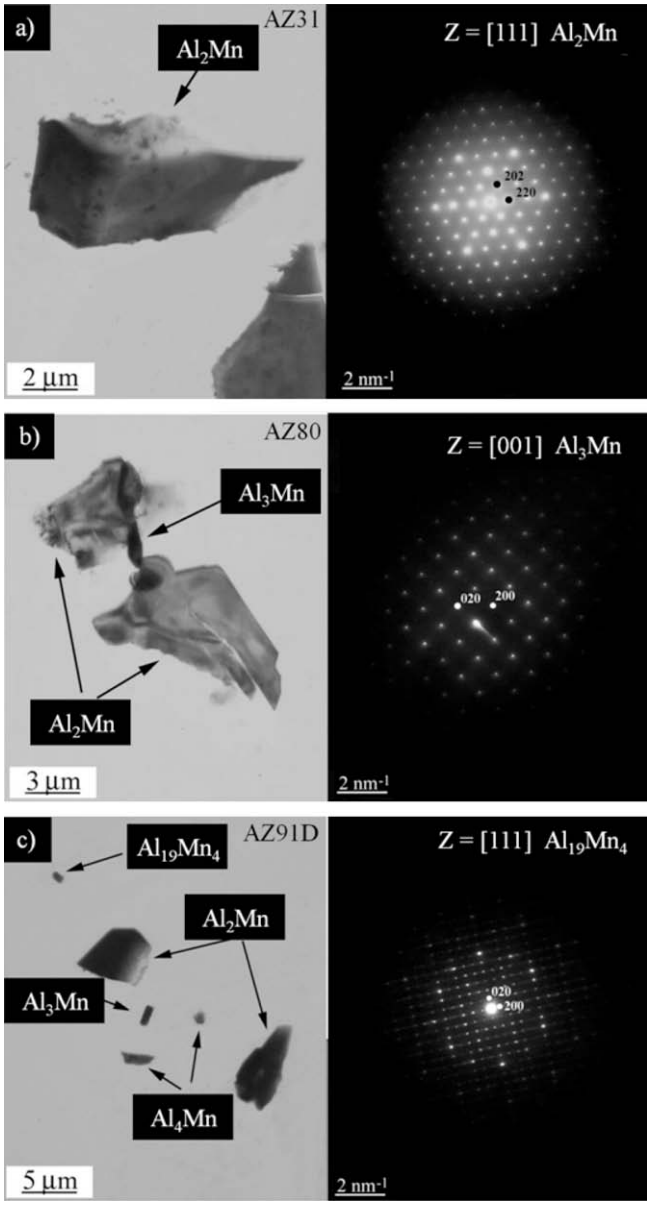

Fig. 2. Transmission electron micrographs and electron diffraction patterns of Al–Mn second phase particles in the (a) AZ31, (b) AZ80 and (c) AZ91D magnesium alloys.

Table 3
Identified Al–Mn second phase particles in the AZ31, AZ80 and AZ91D magnesium alloys.

Material	Particle types
AZ31	$Al_{19}Mn_4$, $Al_{11}Mn_4$, Al_2Mn, Al_8Mn_5
AZ80	$Al_{10}Mn_3$, Al_3Mn, Al_2Mn, Al_8Mn_5
AZ91D	$Al_{19}Mn_4$, Al_4Mn, Al_3Mn, $Al_{11}Mn_4$, Al_2Mn, Al_8Mn_5

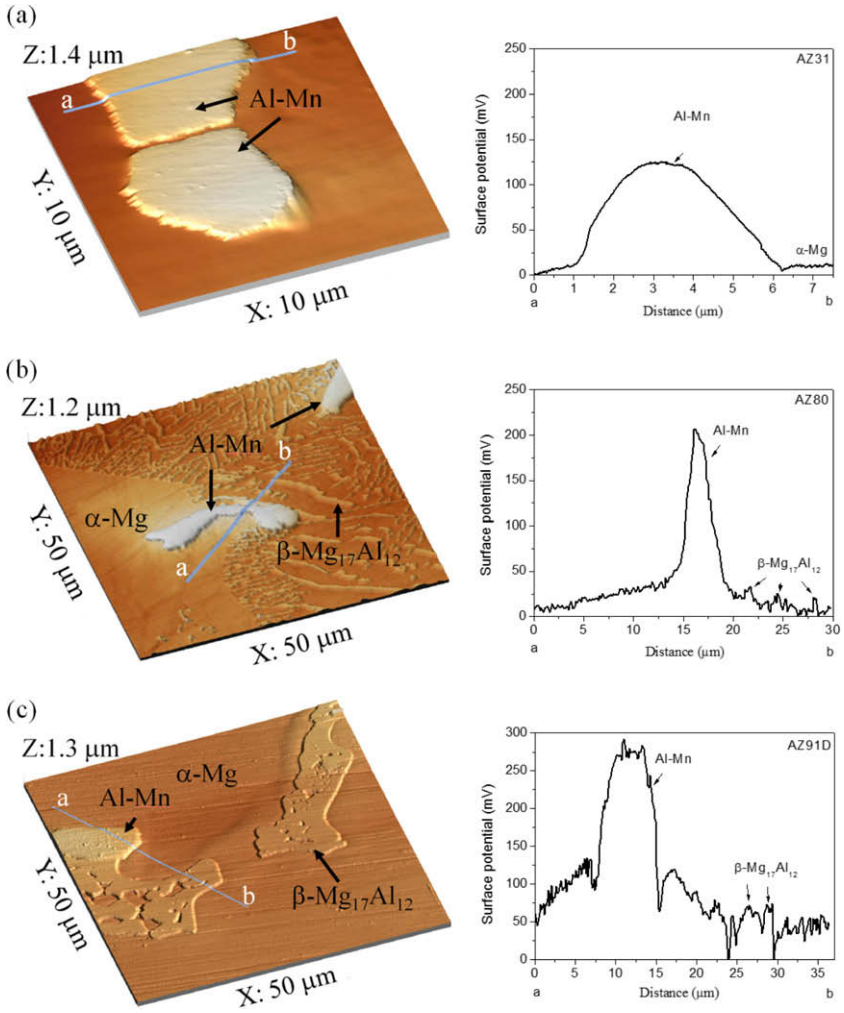

Fig. 3. Topographic images and surface potential profiles of (a) AZ31, (b) AZ80 and (c) AZ91D magnesium alloys.

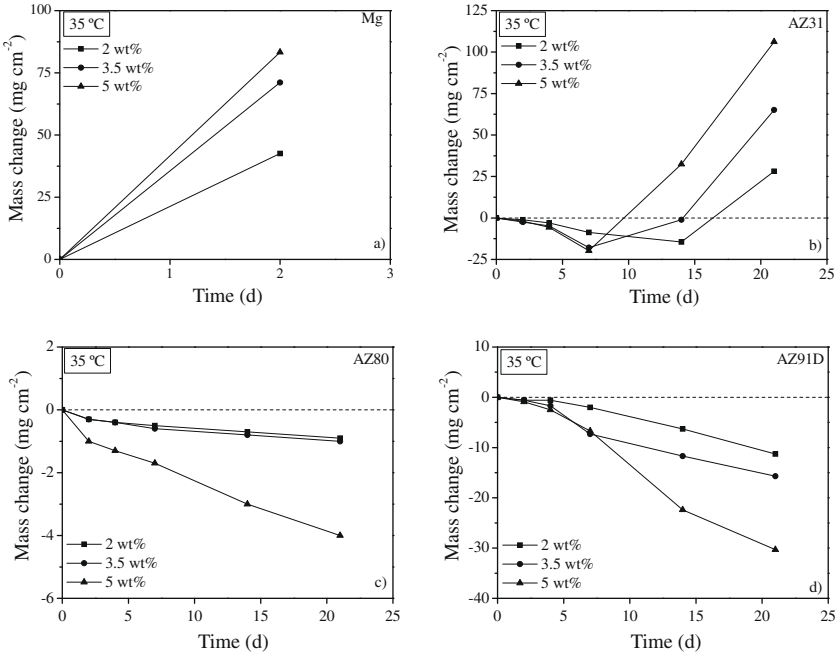

Fig. 4. Mass change *vs.* time of tested materials exposed to a salt fog environment at 35 °C: (a) Mg, (b) AZ31, (c) AZ80 and (d) AZ91D.

Table 4
Kinetic laws of the materials exposed to salt fog (2–3.5–5 wt.% NaCl) environment at 20 °C and 35 °C.

Material	NaCl (wt.%)	Kinetic laws: $y = b \cdot t$; [y (mg cm^{-2}), t(d)]					
		20 °C			35 °C		
Mg	2	$y = 14.55 \times t$	$0 \leqslant t \leqslant 4$	$r^2 = 0.98$	$y = 38 \times t$	$0 \leqslant t \leqslant 2$	$r^2 = 1$
	3.5	$y = 24.55 \times t$	$0 \leqslant t \leqslant 4$	$r^2 = 0.96$	$y = 50 \times t$	$0 \leqslant t \leqslant 2$	$r^2 = 1$
	5	$y = 34.32 \times t$	$0 \leqslant t \leqslant 4$	$r^2 = 0.98$	$y = 55 \times t$	$0 \leqslant t \leqslant 2$	$r^2 = 1$
AZ31	2	$y = -0.45 \times t$	$0 \leqslant t \leqslant 21$	$r^2 = 0.97$	$y = 5.98 \times t$	$14 \leqslant t \leqslant 21$	$r^2 = 1$
	3.5	$y = -1.12 \times t$	$0 \leqslant t \leqslant 21$	$r^2 = 0.98$	$y = 6.07 \times t$	$7 \leqslant t \leqslant 21$	$r^2 = 0.95$
	5	$y = -1.39 \times t$	$0 \leqslant t \leqslant 21$	$r^2 = 0.99$	$y = 8.72 \times t$	$7 \leqslant t \leqslant 21$	$r^2 = 0.99$
AZ80	2	$y = -0.003 \times t$	$0 \leqslant t \leqslant 21$	$r^2 = 0.97$	$y = -0.04 \times t$	$0 \leqslant t \leqslant 21$	$r^2 = 0.96$
	3.5	$y = -0.045 \times t$	$0 \leqslant t \leqslant 21$	$r^2 = 0.98$	$y = -0.04 \times t$	$0 \leqslant t \leqslant 21$	$r^2 = 0.93$
	5	$y = -0.069 \times t$	$0 \leqslant t \leqslant 21$	$r^2 = 0.99$	$y = -0.18 \times t$	$0 \leqslant t \leqslant 21$	$r^2 = 0.98$
AZ91D	2	$y = -0.09 \times t$	$0 \leqslant t \leqslant 21$	$r^2 = 0.98$	$y = -0.54 \times t$	$0 \leqslant t \leqslant 21$	$r^2 = 0.98$
	3.5	$y = -0.19 \times t$	$0 \leqslant t \leqslant 21$	$r^2 = 0.99$	$y = -0.80 \times t$	$0 \leqslant t \leqslant 21$	$r^2 = 0.99$
	5	$y = -0.25 \times t$	$0 \leqslant t \leqslant 21$	$r^2 = 0.98$	$y = -1.55 \times t$	$0 \leqslant t \leqslant 21$	$r^2 = 0.99$

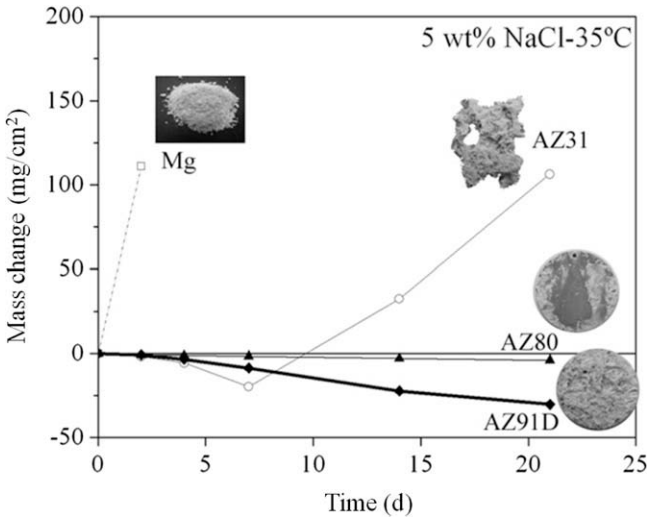

Fig. 5. Comparative study of the mass change of four tested materials (5 wt.% NaCl-35 °C).

3.2. Gravimetric measurements

Fig. 4 shows mass change versus time of test materials exposed to salt fog environment at 35 °C with three different NaCl concentrations (2, 3.5 and 5 wt.%). Unalloyed Mg revealed the fastest degradation with complete disintegration of the specimen after 2 days of exposure (Fig. 4a). For the three tested saline concentrations, the AZ31 alloy (3 wt.% Al) revealed mass gain during the first 4 days, associated with formation of corrosion products of white colour on the surface, and then gradual mass loss until the end of the test, indicating low adhesion of the corrosion products (Fig. 4b). The AZ80 and AZ91D alloys exhibited slightly continuous mass gain during the entire test due to accumulation of corrosion products on the surface. From visual observation of the specimens, the corrosion products were more compact and adherent than those observed in the AZ31 alloy. The effect of the saline concentration was more evident for the AZ91D compared to the AZ80 alloy (Fig. 4c and d). Similar responses were observed for the experiments performed at 20 °C.

Table 4 shows the kinetic laws calculated from gravimetric data using a linear equation ($y = b \cdot t$; y: mass change; t: time) for exposure times where the mass change followed a linear trend. All the

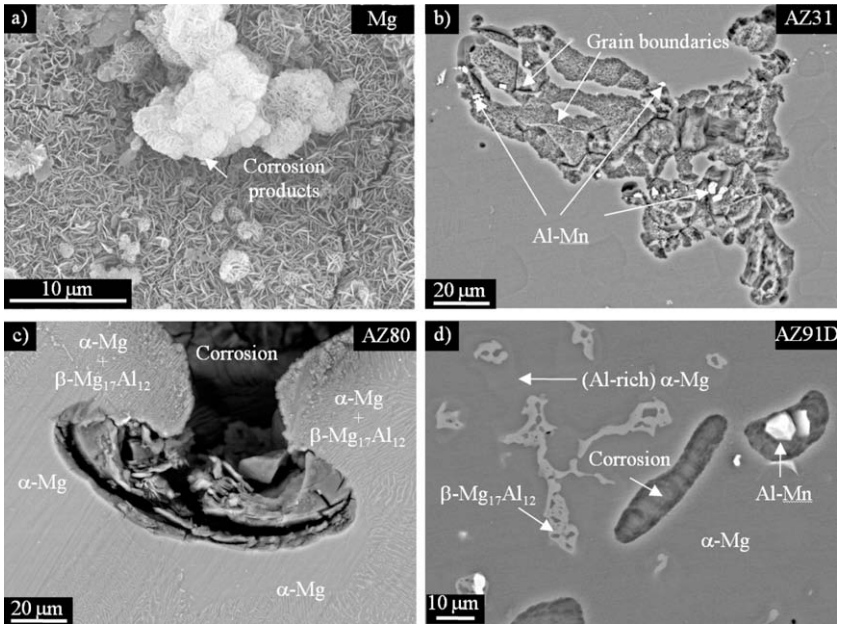

Fig. 6. BSE micrographs after 4 h of exposure to salt fog (5 wt.% NaCl-35 °C) (a) Mg, (b) AZ31, (c) AZ80 and (d) AZ91D.

materials revealed higher kinetic constants with increasing chloride ion concentration and temperature. For instance, the kinetic constant of Mg exposed to salt fog at 35 °C was approximately twice of that observed at 20 °C. The AZ31 alloy revealed two different responses depending on the temperature. At 20 °C, the surface was gradually covered with corrosion products and mass gain was observed during the entire test, whereas at 35 °C, gradual mass loss of the AZ31 alloy was observed due to formation of loose and non-protective corrosion products on the surface. The kinetic constant was considerable reduced for the AZ80 and AZ91D alloys compared with Mg and the AZ31 alloy. For example, the AZ80 alloy revealed kinetic constants 20–150 times lower than those of the AZ31 alloy. In general terms and for the tested conditions, the effect of temperature was more noticeable than that of chloride concentration.

Fig. 5 shows a comparative study of the test materials after exposure to the most aggressive operating conditions used in this work (5 wt.% NaCl, 35 °C). The beneficial effect of aluminium on the corrosion performance of the studied alloys is evident from observation of the gravimetric data and surface appearance after the corrosion test. It is interesting to note that the AZ91D alloy, with the highest aluminium content, revealed higher corrosion attack than the AZ80 alloy. This suggested that the alloy microstructure and/or morphology of the corrosion products played an important role on the corrosion performance of these alloys.

3.3. Morphology and characterization of corrosion products

3.3.1. Early stages of corrosion (4 h)

Fig. 6 illustrates the scanning electron micrographs of plan views of the initial stages of corrosion attack of Mg, AZ31, AZ80 and AZ91D materials after exposure to salt fog for 4 h (5 wt.% NaCl, 35 °C). The entire surface of Mg was covered with voluminous and acicular corrosion products without preferential attack at the grain boundaries (Fig. 6a). The presence of Al–Mn second phase particles in the AZ31 alloy led to localized corrosion in their vicinity, which spread over the surface without formation of deep pits (Fig. 6b). In the case of the AZ80 alloy, the first signs of corrosion were observed in the α-Mg grains (9.7 wt.% Al) with the grains of α + β lamellar aggregate remaining intact (Fig. 6c). The AZ91D alloy revealed preferential corrosion in the centre of the α-Mg dendrites (5.6 wt.% Al) (Fig 6d). Occasionally, corrosion attack was located around the Al–Mn particles situated within the α-Mg dendrites but not around the particles embedded in areas with high aluminium content. *i.e.* β-$Mg_{17}Al_{12}$ and (Al-rich)-α-Mg. Therefore, for the AZ80 and AZ91D alloys exposed to the studied salt fog environments, the Al–Mn particles played a minor role during the early stages of corrosion.

3.3.2. Final stages of corrosion (21 days)

Fig. 7a–c shows the surface morphology of the AZ31, AZ80 and AZ91D materials after exposure to 5 wt.% NaCl salt fog atmosphere for 21 days at 35 °C. The AZ31 alloy revealed general corrosion attack with formation of an uneven corrosion layer, possibly composed of $Mg(OH)_2$ (Fig. 7a). The AZ80 alloy revealed less deterioration, with a small amount of corrosion products on the surface and scattered deep holes or pits, which were possibly associated with preferential corrosion of the α-Mg grains (Fig. 7b). The surface of the AZ91D alloy was completely covered with corrosion products, which appears to be more compact than those formed on the AZ31 alloy (Fig. 7c). The degree of corrosion was less important for the specimens tested at 20 °C, although the morphology of the corrosion products was similar.

Fig. 8 shows the backscattered scanning electron micrographs and X-ray elemental maps of the transversal sections of the AZ31, AZ80 and AZ91D magnesium alloys after 21 days of exposure in 5 wt.% NaCl salt fog at 35 °C. Mg is not shown due to its complete

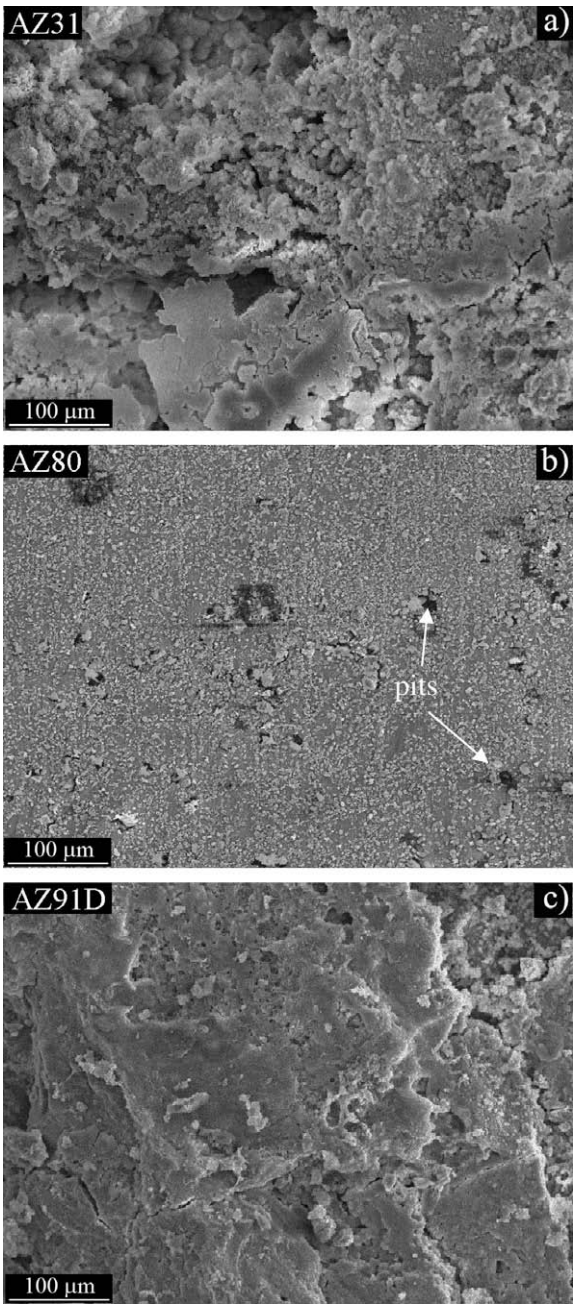

Fig. 7. Scanning electron micrographs of the plan views of test materials after exposure to salt fog (5 wt.% NaCl-35 °C) for 21 days. (a) AZ31, (b) AZ80 and (c) AZ91D.

dissolution after 2 days of test. A thick and loose corrosion layer, possibly consisting of $Mg(OH)_2$, was observed for the AZ31 alloy (Fig. 8a), whereas the AZ80 and AZ91D alloys, with higher aluminium content, revealed lower degree of corrosion. Localized corrosion attack was observed for the AZ80 alloy, which was due to the degradation of the α-Mg grains (Fig. 8b). The grains with the α−β lamellar aggregate revealed minor corrosion with formation of a relatively thin aluminium-rich corrosion layer, which was already observed for the same alloy after immersion in 3.5 wt.% NaCl aqueous solution [25]. Possibly, aluminium enrichment occurred due to preferential dissolution of magnesium. The corrosion attack of the AZ91D alloy advanced through the α-Mg dendrites followed by formation of an uneven corrosion layer that incorporated coarse particles of β-phase. Unlike for the AZ80 alloy, there was not clear

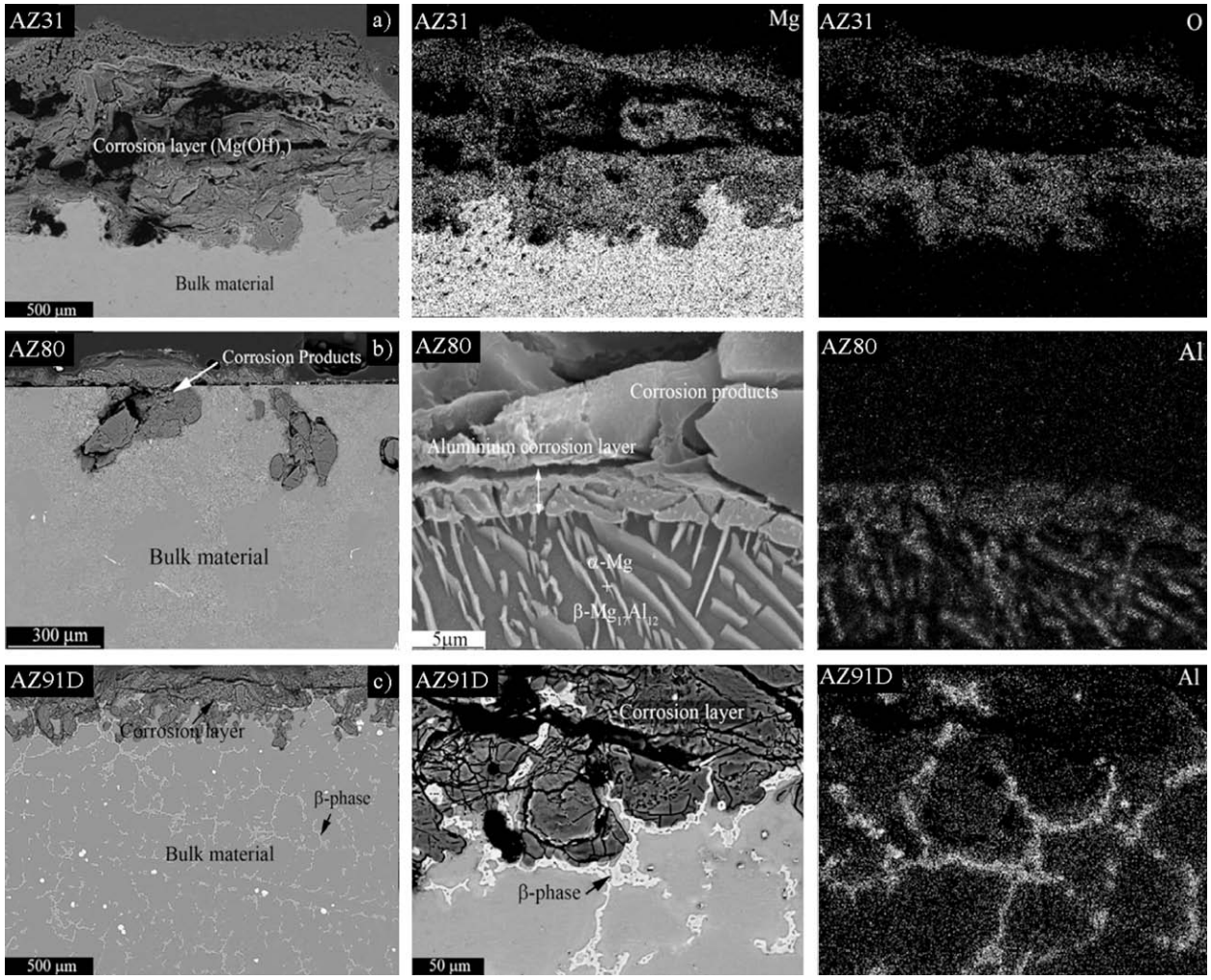

Fig. 8. BSE micrographs and X-ray elemental maps of the cross-sections of (a) AZ31, (b) AZ80 and (c) AZ91D materials after exposure to salt fog (5 wt.% NaCl-35 °C) for 21 days.

evidence of aluminium enrichment on the corrosion products (Fig. 8c).

3.3.3. XRD results

Fig. 9 shows the low angle XRD study (incident angle 1°) of test materials after exposure to salt fog environment for 21 days at 35 °C. The main corrosion product was brucite, $Mg(OH)_2$. Peaks of hydrated magnesium carbonate hydroxide (hydromagnesite $Mg_5(CO_3)_4(OH)_2{\cdot}4H_2O$) were also detected for the AZ alloys, which possibly forms through the reaction of $Mg(OH)_2$ with atmospheric CO_2. The latter showed higher intensity peaks for the AZ80 and AZ91D alloys compared with the Mg and AZ31 materials. Since XRD is limited to crystalline phases, other corrosion products such as nesquehonite ($MgCO_3{\cdot}3H_2O$), magnesium carbonate chloride hydroxide hydrate ($MgCl_2 2MgCO_3(OH)_2{\cdot}6H_2O$, $Mg(OH)_2$ and hydrotalcite ($Mg_6Al_2(OH)_{16}CO_3.4H_2O$) may also be present as amorphous material. Diffraction peaks from the magnesium substrates (Mg and $Mg_{17}Al_{12}$) revealed higher intensity for the specimens exposed to 2 and 3.5 wt.% NaCl (Fig. 9a and b), indicating thinner corrosion layers than those formed after exposure to 5 wt.% NaCl salt fog (Fig. 9c).

4. Discussion

The corrosion behaviour of test materials exposed to salt fog was greatly influenced by their composition and microstructural features. Aluminium content and its distribution in the alloy were the most influencing factors, whereas Al–Mn second phase particles played a secondary role. The findings of the work indicated higher corrosion resistance with increasing aluminium content in the alloy composition, which is typical of Mg–Al alloys exposed to chloride-containing media [26,27]. However, the aluminium distribution and β-phase distribution were found to be crucial for the differences observed between the AZ80 and AZ91D alloys. For the AZ80 alloy, the corrosion attack was located at the α-Mg grains and it was limited when it reached the grains with the lamellar aggregate (α-Mg + β-$Mg_{17}Al_{12}$), due to the fine distribution of the β-phase and to the formation of an aluminium-rich corrosion layer. On the other hand, despite its higher aluminium content, the AZ91D alloy revealed lower corrosion resistance than the AZ80 alloy. Corrosion of the AZ91D alloy initiated at the areas with lower aluminium content, *i.e.* the body of the α-Mg dendrites (5.6 wt.% Al), and the β-phase coarse particles acted as a less efficient electrochemical barrier than the lamellar β-phase in the AZ80 alloy. The formation of an aluminium-rich corrosion layer was not observed for the AZ91D alloy.

A broad range of Al–Mn second phase particles ($Al_{19}Mn_4$, $Al_{11}Mn_4$, Al_8Mn_5...) with iron levels between 0 and 2.5 wt.% were identified by TEM and EDX techniques. The role of these particles on the corrosion behaviour of magnesium alloys depends on many factors, *i.e.* composition, size, etc. Aluminium-rich particles are known [28] to show a relatively low cathodic current density,

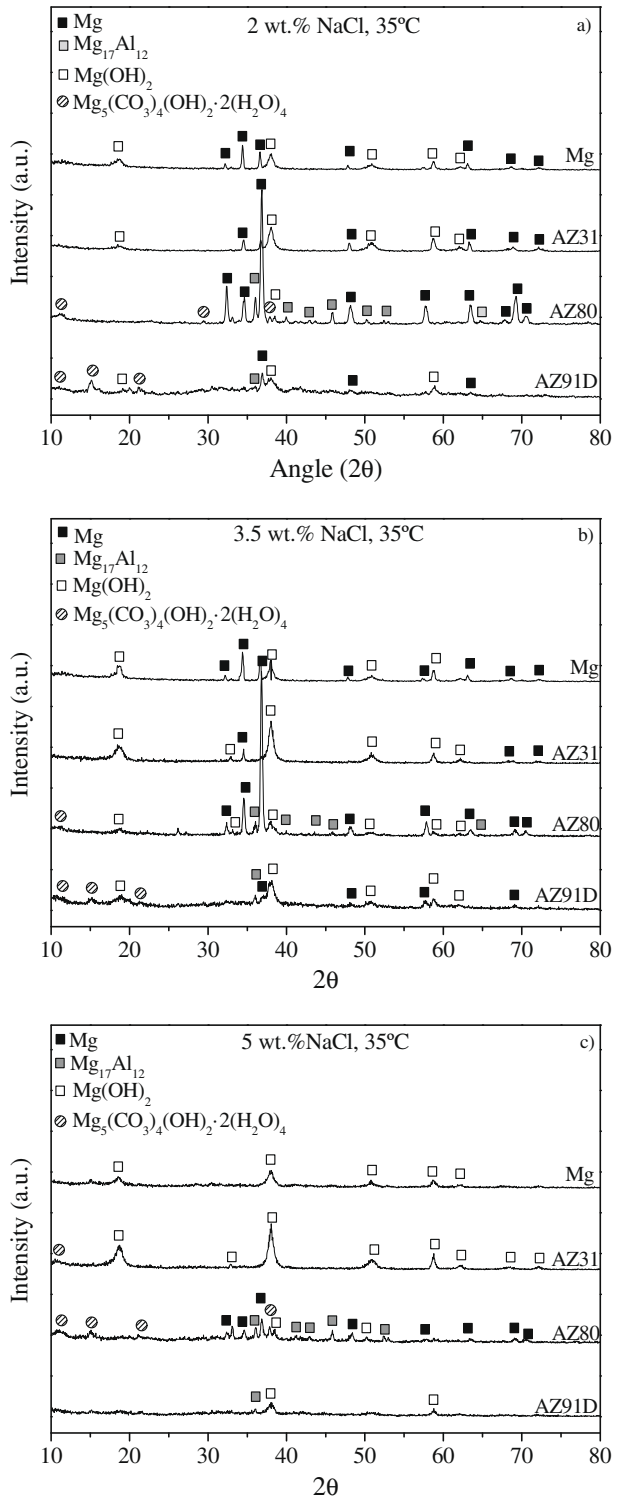

Fig. 9. Low angle XRD patterns (1° incident angle) of corroded specimens after exposure to salt fog environment at 35 °C for 21 days: (a) 2 wt.% NaCl, (b) 3.5 wt.% NaCl and (c) 5 wt.% NaCl.

while those containing high manganese and/or iron can be detrimental to the corrosion resistance of Mg–Al alloys [29]. According to the surface potential maps (Fig. 3), Al–Mn particles exhibit a cathodic behaviour with respect to the magnesium matrix, which was indeed confirmed from observation of the AZ31 alloy after exposition to salt fog for a few hours. However, for the AZ80 and AZ91D alloys, the corrosion mechanism was more influenced by the aluminium distribution and morphology of the more profuse β-phase. Similar features were observed by Jönsson [30] during the atmospheric corrosion of the AZ91D alloy. Previous results of the authors [31] suggested a more important role of the Al–Mn particles when the alloys are immersed in 3.5 wt.% NaCl solution. Therefore, apart from their composition, the role of the Al–Mn particles is also influenced by the alloy in which they are present and the nature of the corrosive medium.

Gravimetric results revealed that the corrosion attack of all test materials increased with the increase in chloride ion concentration. This was possibly associated with increasing breakdown of the partially protective film with increasing chloride ion concentration [32,33]. The results also indicated that the quantity of the increase in corrosion attack was different depending on the alloy. For instance, the effect of the chloride ion concentration was more evident for the AZ91D compared with the AZ80 alloy.

An increase in temperature from 20 to 35 °C also caused an increase in the corrosion attack of Mg, AZ31, AZ80 and AZ91D magnesium materials exposed to salt fog. This behaviour is normally explained by an increase of the kinetics of the electrochemical reactions involved [34].

5. Conclusions

1. Corrosion attack of Mg, AZ31, AZ80 and AZ91D materials under the salt fog test increased with increasing temperature and Cl^- concentration. In general, the effect of temperature was more noticeable than that of chloride concentration. The corrosion attack decreased in the order Mg > AZ31 > AZ91D > AZ80.
2. Al–Mn second phase particles revealed several stoichiometries ($Al_{19}Mn_4$, Al_4Mn, Al_3Mn, $Al_{10}Mn_3$, $Al_{11}Mn_4$, Al_2Mn, Al_8Mn_5) and potential differences up to 300 mV higher than the magnesium matrix. These particles only played a noticeable role in the early stages of corrosion of the AZ31 alloy, facilitating initial corrosion attack at their interface with the magnesium matrix. For the AZ80 and AZ91D alloys, the corrosion behaviour is more influenced by the intense aluminium segregation phenomena generated during the solidification process than by the possible galvanic couples between Al–Mn and β-$Mg_{17}Al_{12}$ phases with the Mg matrix. Thus, corrosion attack commenced at the α-Mg grains and centre of the α-Mg dendrites for the AZ80 and AZ91D alloys respectively. The higher corrosion resistance of the AZ80 alloy compared with the AZ91D alloy was attributed to the finer distribution of the β-phase, which was slightly more noble than the magnesium matrix, and to the formation of an aluminium-rich corrosion layer after protracted times of exposure to the salt fog environment.

Acknowledgements

The authors wish to thank MCYT (Project MAT2009-09845-C02-01) and Comunidad de Madrid (S2009/MAT-1585) for the financial support given to this work.

References

[1] S. Schumann, H. Friedrich, Engineering requirements, strategies and examples, in: H.E. Friedrich, B.L. Mordike (Eds.), Magnesium Technology, Metallurgy, Design Data, Applications, Springer-Verlag, Berlin, Germany, 2006, pp. 499–632.
[2] E. Ghali, W. Dietzel, K. Kainer, General and localized corrosion of magnesium alloys: a critical review, J. Mater. Eng. Perform. 13 (2004) 7–23.
[3] M. Liu, P.J. Uggowitzer, A.V. Nagasekhar, P. Schmutz, M. Easton, G.-L. Song, A. Atrens, Calculated phase diagrams and the corrosion of die-cast Mg–Al alloys, Corros. Sci. 51 (2009) 602–619.
[4] U.C. Nwaogu, C. Blawert, N. Scharnagl, W. Dietzel, K.U. Kainer, Influence of inorganic acid pickling on the corrosion resistance of magnesium alloy AZ31 sheet, Corros. Sci. 51 (2009) 2544–2556.
[5] M.-C. Zhao, P. Schmutz, S. Brunner, M. Liu, G.-L. Song, A. Atrens, An exploratory study of the corrosion of Mg alloys during interrupted salt spray testing, Corros. Sci. 51 (2009) 1277–1292.

[6] G. Ballerini, U. Bardi, R. Bignucolo, G. Ceraolo, About some corrosion mechanisms of AZ91D magnesium alloy, Corros. Sci. 47 (2005) 2173–2184.
[7] L.J. Liu, M. Schlesinger, Corrosion of magnesium and its alloys, Corros. Sci. 51 (2009) 1733–1737.
[8] G. Song, A. Atrens, Understanding magnesium corrosion, Adv. Eng. Mater. 5 (2003) 837–858.
[9] G. Song, A. Atrens, Corrosion mechanisms of magnesium alloys, Adv. Eng. Mater. 1 (1999) 11–33.
[10] R.K.S. Raman, The role of microstructure in localized corrosion of magnesium alloys, Metall. Mater. Trans. A 35 (2004) 2527–2533.
[11] G.L. Makar, J. Kruger, Corrosion of magnesium, Int. Mater. Rev. 38 (1993) 138–153.
[12] G. Song, S. Hapugoda, D. St. John, Degradation of the surface appearance of magnesium and its alloys in simulated atmospheric environments, Corros. Sci. 49 (2007) 1245–1265.
[13] M. Jönsson, D. Persson, D. Thierry, Corrosion product formation during NaCl induced atmospheric corrosion of magnesium alloy AZ91D, Corros. Sci. 49 (2007) 1540–1558.
[14] M. Jönsson, D. Persson, The influence of the microstructure on the atmospheric corrosion behaviour of magnesium alloys AZ91D and AM50, Corros. Sci. (2009), doi:10.1016/j.corsci.2009.11.036.
[15] R. Lindström, L.G. Johansson, J.E. Svensson, The influence of NaCl and CO_2 on the atmospheric corrosion of magnesium alloy AZ91, Mater. Corros. 54 (2003) 587–594.
[16] I.L. Rozenfeld, Atmospheric Corrosion of Metals, NACE, Houston, 1972.
[17] N.D. Tomashov, Theory and Protection of Metals: The Science of Corrosion, The Macmillan Company, New York, 1966.
[18] N.B. Tipton, Salt spray testing, in: Corrosion, ASM Handbook 13, 9th ed., ASM International, Materials Park, OH, 1990.
[19] M.M. Avedesian, H. Baker, ASM Specialty Handbook: Magnesium and Magnesium Alloys, ASM International, Material Park, OH, 1999.
[20] M. Stratmann, H. Streckel, On the atmospheric corrosion of metals which are covered with thin electrolyte layers-I. Verification of the experimental technique, Corros. Sci. 30 (1990) 681–696.
[21] M. Stratmann, H. Streckel, On the atmospheric corrosion of metals which are covered with thin electrolyte layers-II. Experimental results, Corros. Sci. 30 (1990) 697–714.
[22] M. Stratmann, H. Streckel, K.T. Kim, S. Crockett, On the atmospheric corrosion of metals which are covered with thin electrolyte layers-III. The measurement of polarisation curves on metal surfaces which are covered by thin electrolyte layers, Corros. Sci. 30 (1990) 715–734.
[23] W.C. Neil, M. Forsyth, P.C. Howlett, C.R. Hutchinson, B.R.W. Hinton, Corrosion of magnesium alloy ZE41 – The role of microstructural features, Corros. Sci. 51 (2009) 387–394.
[24] M. Jönsson, D. Thierry, N. LeBozec, The influence of microstructure on the corrosion behaviour of AZ91D studied by scanning Kelvin probe force microscopy and scanning Kelvin probe, Corros. Sci. 48 (2006) 1193–1208.
[25] A. Pardo, M.C. Merino, A.E. Coy, F. Viejo, R. Arrabal, S. Feliu Jr., Influence of microstructure and composition on the corrosion behavior of Mg/Al alloys in chloride media, Electrochim. Acta 53 (2008) 7890–7902.
[26] G.L. Makar, K. Kruger, Corrosion studies of rapidly solidified magnesium alloys, J. Electrochem. Soc. 137 (1990) 414–421.
[27] C.B. Baliga, P. Tsakiropoulos, Development of corrosion resistant magnesium alloys. Part 2. Structure of corrosion products on rapidly solidified Mg-16 alloys, Mater. Sci. Technol. 9 (1993) 513–519.
[28] S. Lun Sin, D. Dube, R. Tremblay, Characterization of Al–Mn particles in AZ91D investment castings, Mater. Charact. 58 (2007) 989–996.
[29] R. Zeng, J. Zhang, W. Huang, W. Dietzel, K.U. Kainer, C. Blawert, W. Ke, Review of studies on corrosion of magnesium alloys, Trans. Nonferrous Met. Soc. China 16 (2006) s763–s771.
[30] M. Jönsson, D. Persson, C. Leygraf, Atmospheric corrosion of field-exposed magnesium alloy AZ91D, Corros. Sci. 50 (2008) 1406–1413.
[31] A. Pardo, M.C. Merino, A.E. Coy, R. Arrabal, F. Viejo, E. Matykina, Corrosion behaviour of magnesium/aluminium alloys in 3.5 wt.% NaCl, Corros. Sci. 50 (2008) 823–834.
[32] M.-C. Zhao, M. Liu, G.-L. Song, A. Atrens, Influence of pH and chloride ion concentration on the corrosion of Mg alloy ZE41, Corros. Sci. 50 (2008) 3168–3178.
[33] R. Ambat, N.N. Aung, W. Zhou, Studies of the influence of chloride ion and pH on the corrosion and electrochemical behaviour of AZ91D magnesium alloy, J. Appl. Electrochem. 30 (2000) 865–874.
[34] N. LeBozec, M. Jönsson, D. Thierry, Atmospheric corrosion of magnesium alloys: influence of temperature, relative humidity, and chloride deposition, Corrosion 60 (2004) 356–361.